

The effect of ocean alkalinity and carbon transfer on deep-sea carbonate ion concentration during the past five glacial cycles

Joanna Kerr^{a*} (jk537@cam.ac.uk), Rosalind Rickaby^b (rosalind.rickaby@earth.ox.ac.uk), Jimin Yu^c (jimin.yu@anu.edu.au),

Harry Elderfield^a (he101@cam.ac.uk)

^a Department of Earth Sciences, University of Cambridge, Downing Street, Cambridge, CB2 3EQ, UK. *Corresponding author

^b Department of Earth Sciences, University of Oxford, South Parks Road, Oxford, OX1 3AN, UK

^c Research School of Earth Sciences, Australian National University, Building 142 Mills Road, Acton ACT, 2601, Australia

Abstract

Glacial-interglacial changes in deep Indian and Pacific Ocean carbonate ion concentration ($[\text{CO}_3^{2-}]$) are mainly driven by two mechanisms that operate on different timescales: 1) a long-term increase during glaciation caused by a reduction in carbonate deposition on shelf areas (i.e, the coral reef hypothesis), and 2) transient carbonate compensation responses to changes in deep ocean carbon storage. To investigate these mechanisms, we use benthic B/Ca to reconstruct deep water $[\text{CO}_3^{2-}]$ in cores from the deep Indian and Equatorial Pacific Oceans during the past five glacial cycles. Based on our reconstructions, we suggest that the redistribution of carbonate deposition from shelf areas to the deep ocean raised deep water $[\text{CO}_3^{2-}]$ by 9.2 ± 4.5 (2σ) $\mu\text{mol/kg}$ during glaciations. Oceanic carbon reorganizations during major climatic transitions caused deep water $[\text{CO}_3^{2-}]$ deviations away from the long-term trend and carbonate compensation processes subsequently acted to restore new steady state conditions. Glacial-interglacial trends in $[\text{CO}_3^{2-}]$ are generally in good agreement with records of sediment carbonate contents ($\%\text{CaCO}_3$), suggesting that seafloor $\%\text{CaCO}_3$ is dominated by changes in carbonate preservation in deep water at our studied sites.

Key words: Carbonate ion, Alkalinity, Glacial, Carbonate Compensation, Coral Reef Hypothesis

1. Introduction

If more carbon was stored in the glacial deep ocean, an increase in alkalinity (ALK) would be inevitable (Boyle, 1988; Broecker and Peng, 1989). During glaciation, carbon transfer to the deep ocean increases the dissolved inorganic carbon (DIC) content whilst having a much smaller effect on ALK. The net effect is to cause a shift in DIC speciation away from

36 carbonate ion ($[\text{CO}_3^{2-}]$), lowering the seawater carbonate ion saturation state ($\Delta[\text{CO}_3^{2-}] =$
37 $[\text{CO}_3^{2-}] - [\text{CO}_3^{2-}]_{\text{sat}}$), and shallowing the calcite saturation horizon. The decrease in $\Delta[\text{CO}_3^{2-}]$
38 enhances sea floor CaCO_3 dissolution, disrupting the balance between riverine input and
39 seafloor burial of ALK. This would result in a gain in oceanic ALK, which tends to restore
40 the deep ocean carbonate system to a new steady state. During this so-called carbonate
41 compensation process, the ALK increase further boosts carbon sequestration by lowering
42 surface ocean $p\text{CO}_2$ (Boyle, 1988; Broecker and Peng, 1989).

43
44 The ocean ALK inventory is influenced by carbonate and silicate weathering on land and
45 marine CaCO_3 burial (Milliman et al., 1974). Rates of CaCO_3 burial are dictated by coral
46 reef growth on continental shelves and marine plankton deposition in the deep ocean. As a
47 result, modification of the continental shelf area and/or changes in the rate or composition
48 of biological export production will have a profound effect on the whole ocean ALK budget
49 and, by implication, carbon sequestration in the glacial ocean. Both of these have spawned
50 hypotheses for the ALK driven control of deep ocean carbon storage over glacial-
51 interglacial cycles (Archer and Maier-Reimer, 1994; Berger, 1982; Opdyke and Walker,
52 1992). These hypotheses had previously been dismissed, because despite a significant
53 deepening of the calcite saturation horizon in the glacial Pacific Ocean, it shoaled in the
54 glacial Atlantic Ocean (Catubig et al., 1998). Recent deep water $[\text{CO}_3^{2-}]$ reconstructions
55 suggest that glacial ALK was increased in the global ocean (Rickaby et al., 2010; Yu et al.,
56 2013), reviving the idea that a glacial ALK increase played a pivotal role in reducing
57 atmospheric $p\text{CO}_2$. Nevertheless, debate surrounds the driving mechanism(s) and
58 magnitude of the ALK increase (Rickaby et al., 2010; Yu et al., 2013).

59
60 We present three $[\text{CO}_3^{2-}]$ records from the deep Indian and Pacific Oceans. The modern
61 Pacific and Indian Oceans are relatively homogeneous with respect to deep water $[\text{CO}_3^{2-}]$,
62 because at depth $\text{C}_{\text{org}}:\text{CaCO}_3$ re-mineralise at about a 1:1 ratio, yielding a relatively weak
63 water mass aging effect on $[\text{CO}_3^{2-}]$ (Broecker and Sutherland, 2000). Therefore, glacial-
64 interglacial changes in $[\text{CO}_3^{2-}]$ in the deep Indo-Pacific Ocean should be more sensitive to
65 whole ocean carbonate system changes than those in the Atlantic where past water mass
66 reorganisation influences are thought to be strong (e.g., Curry & Oppo, 2005; Yu et al.,
67 2008). Coupled with benthic $\delta^{13}\text{C}$ and sediment carbonate contents ($\%\text{CaCO}_3$), our $[\text{CO}_3^{2-}]$
68 records place important constraints on how the global carbon cycle changed over glacial-

interglacial cycles. We show two records that are sufficiently well resolved to define shifts in $[\text{CO}_3^{2-}]$ through five glacial-interglacial cycles, and one high-resolution record that allows confident assessment of carbonate compensation processes over the last full glacial cycle. Together, these afford a robust insight into the mechanisms driving deep ocean $[\text{CO}_3^{2-}]$ on glacial-interglacial timescales.

2. Core locations and methods

2.1 Core locations

Site WIND 28K is located at 4.2 km water depth in the Western Indian Ocean Mascarene Basin (Fig.1, Table 1). Guided by prominent seafloor bathymetry, southern sourced Circumpolar Deep Water (CDW) ventilates the deep Western Indian Ocean (Toole and Warren, 1993). The Weddell Sea contributes to the densest waters found in the western basin, and above this, deep and intermediate waters enter from both the south and north.

Site TT013-PC72 is situated in the deep Equatorial Pacific Ocean at 4.3 km water depth, and site ODP 806 is located at 2.5 km water depth on the northeast margin of the Ontong Java Plateau (Fig. 1, Table 1). The latter core is located above the modern ocean calcite saturation horizon which lies at ~ 3 km water depth. The Ontong Java Plateau straddles the equator in the Western Pacific Ocean, covering an area of 1000 km by 1500 km, and rising to uncharacteristically shallow depths of ~ 1.7 km.

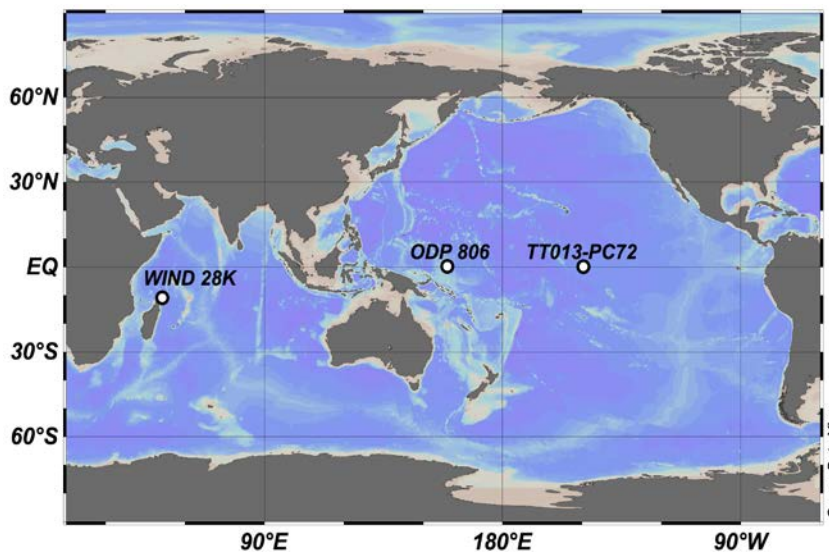


Figure 1: Location of sediment cores in the Indian Ocean (WIND 28K) and Pacific Ocean (ODP 806, TT013-PC72).

102

Core	Latitude (°N)	Longitude (°E)	Water Depth (km)	[CO ₃ ²⁻] (μmol/kg)	[CO ₃ ²⁻] _{sat} (μmol/kg)
WIND 28K	-10.9	51.5	4.2	84	95
ODP 806	0.2	159.2	2.5	73	69
TT013-PC72	0.1	-149.4	4.3	80	98

103

104

105

Table 1: Location and depth of sediment cores, in situ [CO₃²⁻] (μmol/kg) and calcitic [CO₃²⁻]_{sat} (μmol/kg). Seawater [CO₃²⁻] is calculated using GLODAP and WOA13 gridded data (Key et al., 2004) using the CO₂sys.xls model (Pelletier et al., 2005).

106 2.2 Methods

107

108 Sediment samples of ~10 cm³, from 2 cm segments, were disaggregated in deionized
 109 water and wet sieved through 63 μm sieves. Since no size effect on B/Ca is found
 110 (Supplementary Material 1), we have picked pristine *Cibicidoides wuellerstorfi* (*C.*
 111 *wuellerstorfi*) tests from all size fractions ranging from 180 to 500 μm. Shells were gently
 112 crushed between two glass plates and cleaned according to Barker et al. (2003). The
 113 reductive cleaning step was not included in the cleaning, as no cleaning effect is observed
 114 between different cleaning methods (Yu et al., 2007, G3).

115

116 Trace element ratios of cleaned foraminifera shells were determined by Quadrupole ICP-
 117 MS or Thermo® Element XR HR-ICP-MS at the University of Cambridge, according to Yu et
 118 al. (2005) and Misra et al. (2014), respectively. The long-term precision of B/Ca measured
 119 using in-house standard solutions by Quadrupole ICP-MS is 153.29 ± 7.56 μmol/mol or
 120 4.93% (2σ, n = 88), and by HR-ICP-MS is 198.59 ± 6.97 μmol/mol or 3.51% (2σ, n = 144).
 121 The latter translates into an uncertainty of ± 5.71 μmol/kg (2σ) in the reconstructed bottom
 122 water [CO₃²⁻]. Full details of sample preparation and analytical methods are given in
 123 Supplementary Material 2.

124

125 Deep water [CO₃²⁻] is reconstructed from B/Ca changes relative to core-top values
 126 assuming that pre-industrial [CO₃²⁻] is recorded by core-top B/Ca measurements. This
 127 method of calculation eliminates the requirement for an intercept value, which due to the
 128 scatter around the regression line of B/Ca and Δ[CO₃²⁻] (Yu and Elderfield, 2007), can
 129 cause an offset between core-top and pre-industrial Δ[CO₃²⁻]. This approach was first
 130 implemented by Yu et al. (2008) and later discussed in detail by Yu et al. (2016). The widely

131 applied linear sensitivity of the B/Ca in *C. wuellerstorfi* to $\Delta[\text{CO}_3^{2-}]$ of Yu and Elderfield
132 (2007) has been adjusted to account for systematic offsets in internal laboratory standards
133 (Supplementary Material 3) :

134

$$135 \quad \Delta[\text{CO}_3^{2-}]_{\text{downcore}} = \Delta[\text{CO}_3^{2-}]_{\text{pre-industrial}} + \Delta\text{B/Ca} / 1.25$$

136

137 $\Delta[\text{CO}_3^{2-}]_{\text{pre-industrial}}$ is calculated by removing the anthropogenic influence on
138 $\Delta[\text{CO}_3^{2-}]$ using the GLODAP dataset (Key et al., 2004), and $\Delta\text{B/Ca}$ represents the deviation
139 of down-core B/Ca values from the core-top value. Note that this slope modification has
140 negligible effect on previous deep water $[\text{CO}_3^{2-}]$ reconstructions, as both core-top and
141 downcore samples were measured by the same set of calibration standards (Yu &
142 Elderfield, 2007; Yu et al, 2010, Rickaby et al., 2010).

143

144 Due to a lack of core-top data from WIND 28K and ODP 806, B/Ca values from Yu et al.
145 (2010a) have been used for WIND 28K and the core-top B/Ca for a nearby core MW91-9-
146 GGC15 (Yu et al., 2013) for ODP 806. Data from Yu et al. (2010a) and Yu et al. (2013)
147 have also been adjusted to account for the offset in internal laboratory standards
148 (Supplementary Material 3). Core top ages range from 3.65 ka to 5.40 ka, therefore there
149 may be inaccuracies in absolute $[\text{CO}_3^{2-}]$ values, however this would have little impact on
150 our interpretation which mainly relies on the B/Ca pattern downcore.

151

152 Changes in $[\text{CO}_3^{2-}]_{\text{sat}}$ are primarily driven by pressure, with little influence from temperature
153 and salinity changes. As a result, $[\text{CO}_3^{2-}]_{\text{sat}}$ remains roughly stable on glacial-interglacial
154 timescales (Yu et al., 2008), and pre-industrial $[\text{CO}_3^{2-}]_{\text{sat}}$ can be used alongside
155 reconstructed $\Delta[\text{CO}_3^{2-}]$ to calculate $[\text{CO}_3^{2-}]$ by:

156

$$157 \quad [\text{CO}_3^{2-}] = \Delta[\text{CO}_3^{2-}] + [\text{CO}_3^{2-}]_{\text{sat}}$$

158

159 Gridded GLODAP (Key et al., 2004) and WOA13 data were used to constrain bottom water
160 temperature, salinity, total [P], total [Si], ALK, and pre-anthropogenic TCO_2 . Pre-industrial
161 $[\text{CO}_3^{2-}]$ and calcite saturation state (Ω) were then calculated using CO2sys.xls model
162 (Pelletier et al., 2005). Equilibrium constants K_1 and K_2 for carbonic acid were taken from

Mehrbach (1973), refit by Dickson & Millero (1987), K_{SO_4} is from Dickson (1990), and $[\text{B}]_{\text{total}}$ from Uppstrom (1974).

2.3 Age models

The age models for ODP 806 and TT013-PC72 have been constructed by aligning *C. wuellerstorfi* $\delta^{18}\text{O}$ to the LR04 global benthic $\delta^{18}\text{O}$ stack (Lisiecki and Raymo, 2005). The age model of Johnstone et al., (2014) for WIND 28K has also been extended using this method. Tie points were identified and linear interpolation was applied between these tie points. All core locations capture the expected glacial-interglacial range in benthic $\delta^{18}\text{O}$ with little evidence of strong 'smoothing'. We do not believe that our interpretations are significantly compromised by bioturbation, although we practice caution when investigating short-term changes down-core. Full details of each age model are shown in Supplementary Material 4.

3. Results and discussion

Figure 2 shows reconstructed deep-sea $[\text{CO}_3^{2-}]$ over glacial-interglacial cycles at three sites. Two distinct trends are shared by all three $[\text{CO}_3^{2-}]$ records: 1) long-term increases parallel to a decline in atmospheric $p\text{CO}_2$ and global sea level, and 2) transient excursions off the long-term increase. We suggest that these trends are driven by two separate mechanisms.

3.1 Glacial increase in alkalinity

The most striking feature is the long-term glacial increase in $[\text{CO}_3^{2-}]$ that is seen in all three deep Indian and Pacific Ocean records over several glacial cycles (Fig. 2). As previously discussed, dissolution of seafloor CaCO_3 associated with greater carbon storage in the glacial deep ocean would raise deep ocean $[\text{CO}_3^{2-}]$, however we suggest that this is not the driving mechanism for the long-term $[\text{CO}_3^{2-}]$ increase. Carbonate compensation processes would act to bring conditions back to steady state on a time scale of ~ 7 kyr, not leading to a long-term change as observed in our records. thus if whole ocean ALK is unchanged, deep ocean $[\text{CO}_3^{2-}]$ would not be greatly different to Holocene values. Furthermore, if dissolution

196 of seafloor CaCO_3 alone were driving the glacial $[\text{CO}_3^{2-}]$ increase, a simultaneous decline in
197 $\%\text{CaCO}_3$ would be expected. In contrast, seafloor CaCO_3 preservation follows similar
198 trends to deep-ocean $[\text{CO}_3^{2-}]$ at all three sites, and peaks during MIS 3 at WIND 28K (Fig.
199 3). It is worth noting that glacial-interglacial changes in CaCO_3 preservation in the deep
200 Pacific Ocean are not complicated by dilution by lithogenic materials. Anderson et al. (2008)
201 used the ^{230}Th normalization technique to show that the preserved CaCO_3 flux at TT013-
202 PC72 was higher during glacial periods compared to interglacial periods. Furthermore,
203 aeolian dust supply (a major source of lithogenic material to the Central Pacific Ocean) was
204 greater during glacial periods (Winckler et al., 2008), thus

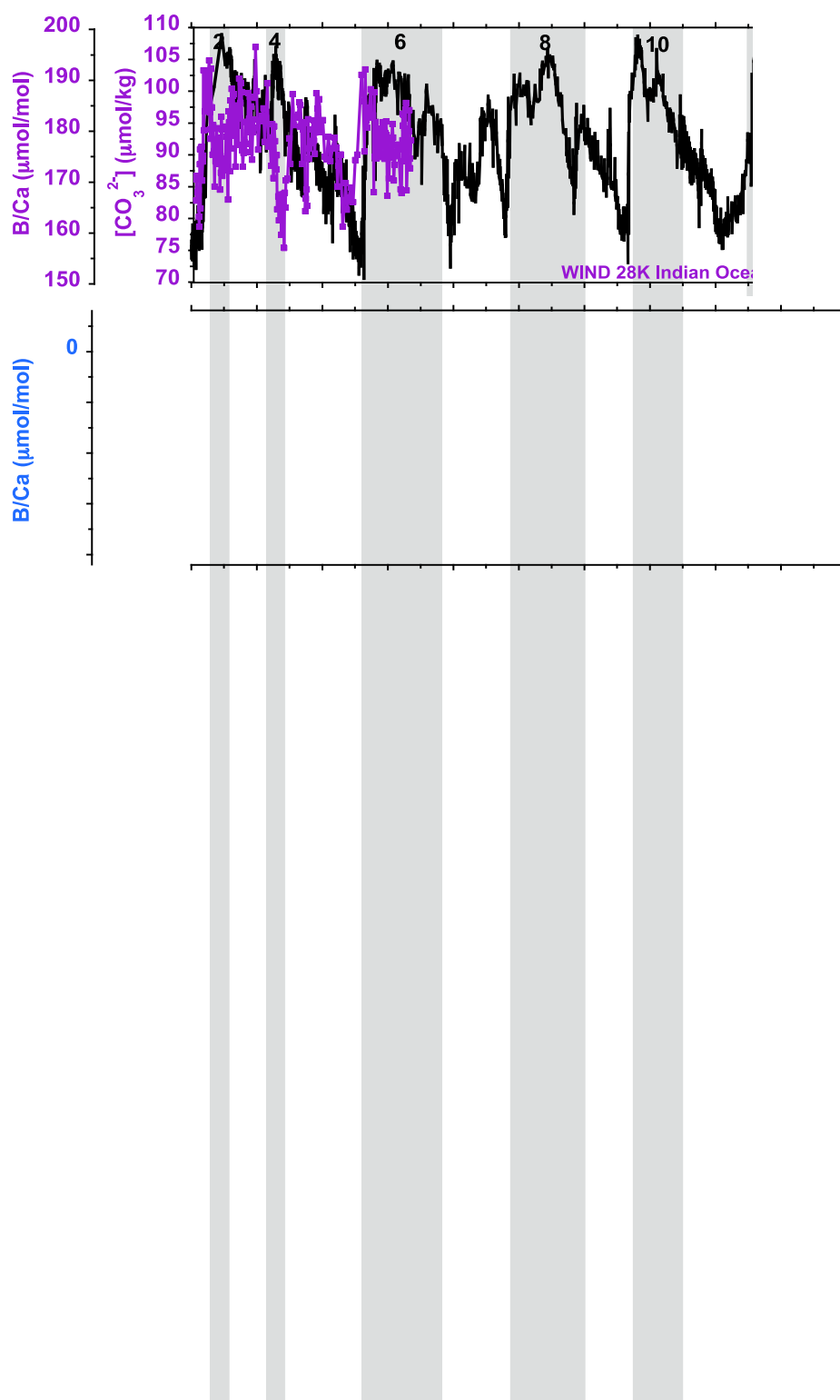


Figure 2: Changes in $[CO_3^{2-}]$ at A) WIND 28K (purple), B) ODP 806 (blue), and C) TT013-PC72 (red). Relative Sea Level (RSL) is given in black (Grant et al., 2012, 2014). D) 10ky moving average of $[CO_3^{2-}]$ at sites WIND 28K (purple), ODP 806 (blue), and TT013-PC72 (red) on left y axis, and RSL record (black) on right y axis. E) Atmospheric CO_2 (Lüthi et al., 2008; Monnin et al., 2001; Petit et al., 1999; Siegenthaler et al., 2005). Grey bars show Marine Isotope Stages. WIND 28K data from <47.9 ka are from Yu et al., (2010a).

aCO_3 dissolution
 CaCO_3 burial

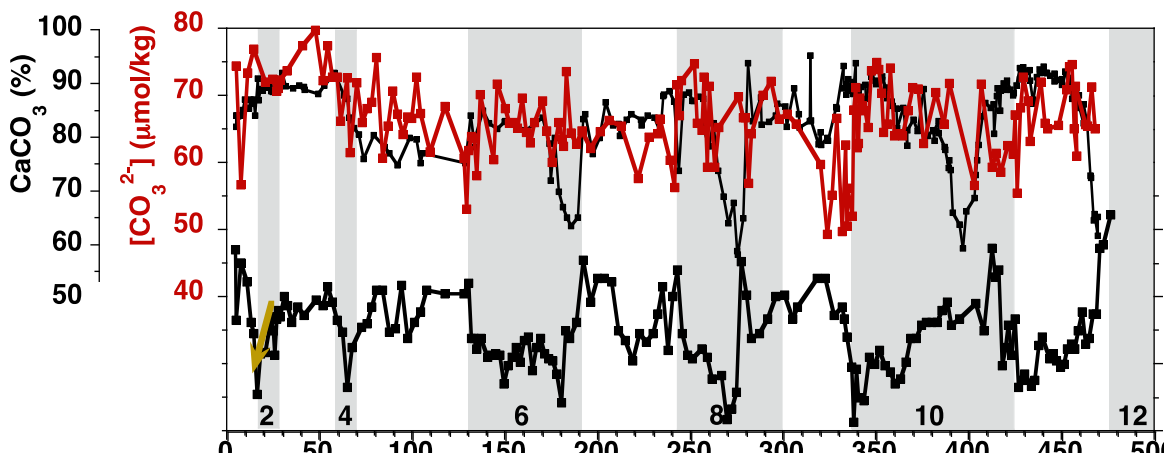


Figure 3: Deep water $[\text{CO}_3^{2-}]$ ($\mu\text{mol/kg}$) and $\delta^{13}\text{C}$ (‰) from A) WIND 28K B) ODP 806, C) TT013 PC72. Arrows illustrate the direction of $[\text{CO}_3^{2-}]$ and $\delta^{13}\text{C}$ changes at key intervals and the processes thought to be driving the change: carbon addition to deep ocean (yellow), carbon removal from deep ocean (green), CaCO_3 dissolution (red), and CaCO_3 burial (blue) (see text for full description of the driving processes). Grey bars show Marine Isotope Stages. WIND 28K $[\text{CO}_3^{2-}]$ data (<47.9 ka) are from Yu et al. (2010a), $\delta^{13}\text{C}$ data are from McCave et al. (2005) for WIND 28K, Bickert et al. (1993) and this study for ODP 806 and courtesy of Alan Mix for TT013-PC72. CaCO_3 (%) data are from McCave et al. (2005) for WIND 28K, Janecek (1993) and this study for ODP 806, and Anderson et al., (2008) for TT013-PC72.

207 dilution would cause a glacial minima in %CaCO₃. Comparison of the [CO₃²⁻] record with
 208 the ²³⁰Th-normalised CaCO₃ accumulation rate at site TT013-PC72, shows that higher
 209 [CO₃²⁻] was associated with a greater preserved flux of CaCO₃ (Fig. 4). This supports the
 210 growing consensus that the seafloor CaCO₃ content is mainly controlled by deep-sea
 211 preservation (refs; Anderson et al., Yu et al., 2013). In detail, the relationship is not linear as
 212 carbonate accumulation records a step change to higher carbonate accumulation, while
 213 deep ocean [CO₃²⁻] records a more gradual increase during glaciation (Fig. 4). Anderson et
 214 al. (2008) showed that the CaCO₃ flux is unlikely to be controlled by changes in surface
 215 productivity, therefore we suggest that this discrepancy may be explained by the non-linear
 216 dynamics of CaCO₃ dissolution in the deep ocean. In the modern ocean, the saturation
 217 state is coupled with the depth of the ‘snow line’ – the transition from a seafloor covered in
 218 calcite to an almost calcite-free seafloor. This transition is gradual, with the depth at which
 219 calcite begins to rapidly dissolve known as the calcite saturation horizon and the depth at
 220 which there is no net accumulation of CaCO₃ known as the carbonate compensation depth
 221 (CCD). Since site TT013-PC72 is located close the modern CCD (Broecker, 2008,
 222 paleoceanography), an increase in ambient [CO₃²⁻] and/or an increase in surface
 223 productivity (or export production) would be required to increase sediment %CaCO₃. More
 224 records of the preserved CaCO₃ flux and ambient [CO₃²⁻] from a range of water depths in
 225 the deep Indo-Pacific Ocean are required to test the exact mechanism, however this will not
 226 significantly affect the conclusion that the deep ocean [CO₃²⁻] rise during glaciation is not
 227 driven by dissolution of seafloor CaCO₃ in the Pacific Ocean.

228

229

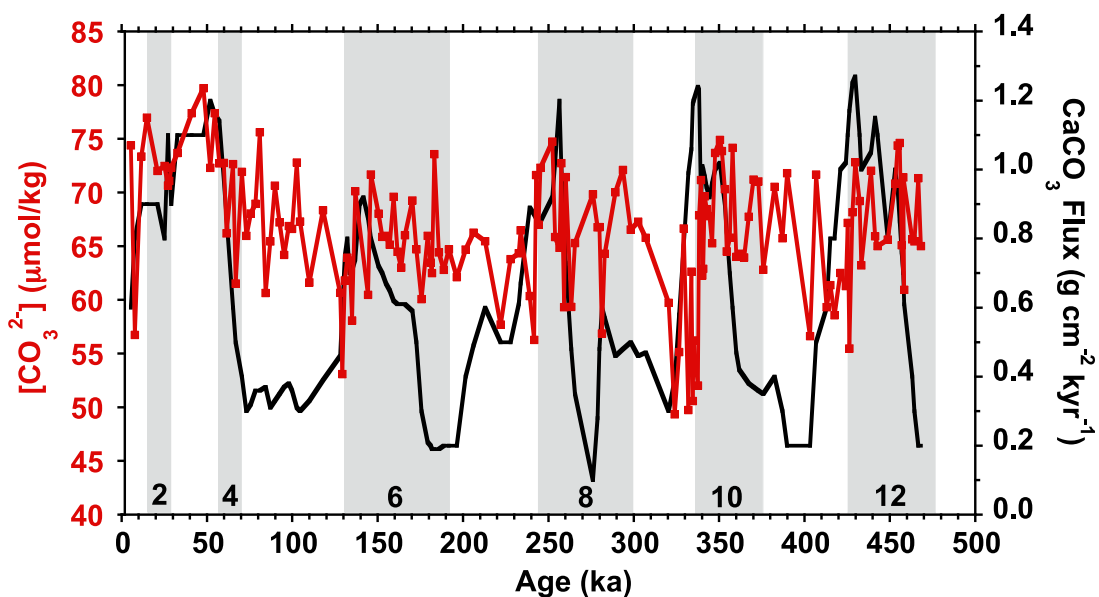
230

231

232

233

234



10
Figure 4: Deep water [CO₃²⁻] (μmol/kg) and CaCO₃ flux (g cm⁻² y⁻¹) at site TT013-PC72 over the last 500 ky. CaCO₃ flux data are from Anderson et al. (2008). Marine Isotope Stages are represented by grey bars.

236 An increase in the glacial organic carbon (C_{org}) to $CaCO_3$ export ratio ($C_{org}:CaCO_3$) would
 237 elevate deep ocean ALK by enhancing dissolution of seafloor $CaCO_3$ in pore waters
 238 (Archer and Maier-Reimer, 1994). However, if an increase in the $C_{org}:CaCO_3$ rain ratio was
 239 driving the $[CO_3^{2-}]$ increase, initial decreases in both deep-water $[CO_3^{2-}]$ and $\delta^{13}C$ would be
 240 expected but this is not observed in our records (Fig. 3). Furthermore, $[CO_3^{2-}]$ would be
 241 expected to be much higher at the Last Glacial Maximum (LGM) than the modern value,
 242 which is not the case. We suggest that a change in the $C_{org}:CaCO_3$ export ratio is not
 243 driving the long-term glacial $[CO_3^{2-}]$ increase in the deep Indian or Pacific Ocean, however
 244 we acknowledge that identifying changes in the $C_{org}:CaCO_3$ export ratio from $[CO_3^{2-}]$ and
 245 $\delta^{13}C$ in the deep ocean alone is difficult as $[CO_3^{2-}]$ is influenced by a number of other
 246 factors.

247 Preservation of seafloor $CaCO_3$ acts to reduce an increase in ocean ALK and hence
 248 maintain the oceanic carbonate system at steady state. Therefore, in order to increase
 249 deep-ocean $[CO_3^{2-}]$ and promote seafloor $CaCO_3$ preservation, glacial ALK must have
 250 been higher than modern ocean conditions. The major sources and sinks of ocean ALK are
 251 weathering of terrestrial carbonates and silicates, and marine $CaCO_3$ burial, respectively
 252 (Milliman et al., 1974). $CaCO_3$ burial takes place both in the deep ocean by marine plankton
 253 burial, and on continental shelves via coral reef growth. In the modern ocean, shallow water
 254 carbonate production accounts for approximately half of global $CaCO_3$ burial (Milliman,
 255 1993; Opdyke and Walker, 1992). During glaciation, sea level drop would reduce the shelf
 256 area, consequently leading to a decrease in $CaCO_3$ burial on continental shelves.
 257 Assuming no change in ALK input due to terrestrial weathering, a reduction in glacial sea
 258 level would increase the ocean ALK inventory and hence increase deep ocean $[CO_3^{2-}]$. We
 259 suggest that the long-term rise in deep ocean $[CO_3^{2-}]$ is consistent with reduced $CaCO_3$
 260 deposition on shelf areas, associated with the sea level drop during glaciation, i.e. the coral
 261 reef hypothesis (Berger, 1982; Opdyke and Walker, 1992). There is also a hint in the WIND
 262 28K data that the $[CO_3^{2-}]$ rise from stage 5d to 5a could be driven by the carbonate system
 263 re-attaining steady state after the excess carbonate burial during the sea-level rise and
 264 highstand of the termination to 5e conditions (Fig. 2).

265 A reduction in glacial sea level will also expose $CaCO_3$ rich shelf areas to chemical
 266 weathering. Shelf carbonates tend to weather at a faster rate than other rock types,

267 potentially increasing ocean ALK further than the CaCO_3 shelf-to-basin shift alone (Gibbs
268 and Kump, 1994). However, substantial research suggests that decreased temperatures
269 and precipitation during glacial periods acted to reduce rates of chemical erosion, resulting
270 in negligible glacial-interglacial variation in the global weathering rates (Foster and Vance,
271 2006; Munhoven, 2002). Given the global nature of the long-term ALK increase shown by
272 our data we suggest that redistribution of shelf ALK to the deep ocean is the most plausible
273 explanation.

274 The 'coral reef' hypothesis had been ruled out as the mechanism controlling atmospheric
275 CO_2 during glacial periods, because despite a deepening of the saturation horizon in the
276 glacial Pacific Ocean, it shoaled in the Atlantic Ocean (Catubig et al., 1998). However, we
277 suggest that if the rate of glacial carbon sequestration was sufficiently high in the deep
278 Atlantic Ocean, this could have countered the $[\text{CO}_3^{2-}]$ rise that would be driven by the
279 global ALK increase. A conservative estimate of carbon storage suggests that the deep
280 Atlantic Ocean sequestered a large amount of carbon, which was, in quantity equivalent to
281 $\sim 86 \pm 56$ % of the carbon lost from the atmosphere during the MIS 5-4 transition (Yu et al.,
282 2016). Therefore, deep Atlantic Ocean carbon storage that is sufficient to drive a reduction
283 in deep ocean $[\text{CO}_3^{2-}]$ on a background of globally elevated ocean ALK is possible.

284 A net gain in whole ocean ALK decreases atmospheric CO_2 by shifting DIC distribution
285 away from $\text{CO}_{2(\text{aq})}$. A considerable proportion of the global surface ocean is in equilibrium
286 with the atmosphere, thus any change in surface ocean $[\text{CO}_{2(\text{aq})}]$ is reflected in atmospheric
287 $p\text{CO}_2$. As sea level rises during deglaciation, and neritic CaCO_3 burial is increased, the
288 opposite effects are recorded (Berger, 1982; Opdyke and Walker, 1992).

289 Importantly, a rise in global ocean ALK associated with reduced neritic deposition could
290 account for a reduction in atmospheric $p\text{CO}_2$ prior to any major reorganization of water
291 masses. If we consider the last full glacial cycle, $[\text{CO}_3^{2-}]$ increases by ~ 13 $\mu\text{mol/kg}$ between
292 120-80 ka at site WIND 28K (Fig. 2A), before any major reorganization of water masses at
293 the MIS 5/4 boundary (Adkins, 2013). Globally relative sea level fell by ~ 60 m during MIS 5
294 (Grant et al., 2014), significantly reducing the shelf area for CaCO_3 burial (Fig. 2). If the ALK
295 previously accumulated on shelf at highstand is retained in the ocean for 10 ky, this could
296 increase $[\text{CO}_3^{2-}]$ by ~ 80 $\mu\text{mol/kg}$ (Rickaby et al., 2010). Transfer of shelf ALK to the ocean
297 will likely be accompanied by an increase in the DIC content of the ocean, either by
298 sequestration of CO_2 into surface waters which are subsequently transported to depth, or

299 by transfer of organic carbon from shelf areas to the deep ocean. Assuming a simultaneous
300 addition of 500 PgC along with the ALK addition, the $[\text{CO}_3^{2-}]$ rise would be reduced to ~ 25
301 $\mu\text{mol/kg}$ (Rickaby et al., 2010), which remains more than sufficient to account for the
302 magnitude of $[\text{CO}_3^{2-}]$ increase recorded at all three sites (Section 3.3). Atmospheric CO_2
303 concentrations fell by ~ 50 ppm during MIS 5 (Petit et al., 1999), suggesting that an increase
304 in whole ocean ALK may play a role in driving glacial carbon sequestration to the ocean
305 prior to major changes in water mass organization. Recent model simulations suggest that
306 the combined effects of increased whole ocean ALK and nutrient inventories associated
307 with lowered glacial sea level could account for 51% of the glacial decline in atmospheric
308 $p\text{CO}_2$ (Wallmann et al., 2016).

309 **3.2 Transient changes in $[\text{CO}_3^{2-}]$**

310 Records from the deep Indian and Pacific Oceans display transient $[\text{CO}_3^{2-}]$ changes away
311 from the long-term increasing trend. WIND 28K is the only one of our three records that has
312 sufficiently high resolution to assess these changes in detail. However, similar deviations
313 from the long term trend, that are coincident with transient shifts in higher resolution
314 $\%\text{CaCO}_3$ and/or $\delta^{13}\text{C}$ records, are also recorded at ODP 806 (Fig. 3B). We suggest that
315 these transient shifts are driven by carbonate compensation responses to changes in deep
316 ocean carbon storage, which take place on timescales of ~ 8.5 kyr (Ridgwell and
317 Hargreaves, 2007).

318

319 **3.2.1 Carbon transfer to the deep ocean**

320

321 If more carbon is stored in the deep ocean, all else remaining equal, a carbonate
322 compensation response is inevitable. Carbon transfer from surface and intermediate waters
323 to depth lowers deep-ocean $[\text{CO}_3^{2-}]$ and subsequently promotes dissolution of seafloor
324 CaCO_3 . WIND 28K records a ~ 25 $\mu\text{mol/kg}$ decrease in $[\text{CO}_3^{2-}]$ and $\sim 0.5\text{‰}$ decrease in
325 $\delta^{13}\text{C}$ at the MIS 5 to MIS 4 transition as carbon is transferred to the deep ocean. This
326 $[\text{CO}_3^{2-}]$ decrease is remarkably similar to the change recorded in the deep South Atlantic
327 Ocean at the MIS 5 to MIS 4 transition (Yu et al., 2016), suggesting that a carbon rich
328 southern sourced water mass bathed a large proportion of the global deep ocean at the
329 beginning of MIS 4. As previously discussed, carbon addition to the deep ocean promotes
330 dissolution of seafloor CaCO_3 , increasing $[\text{CO}_3^{2-}]$ to restore steady state conditions. This

process probably explains a portion of the $[\text{CO}_3^{2-}]$ rise from MIS 4 to MIS 3, however the simultaneous rise in $\delta^{13}\text{C}$ suggests that carbonate compensation is not the only driving mechanism (Fig. 3A).

To remove ‘open system’ effects on $\delta^{13}\text{C}$ and $[\text{CO}_3^{2-}]$, the difference between $[\text{CO}_3^{2-}]$ and $\delta^{13}\text{C}$ in the Caribbean Basin (VM28-122, Yu et al. (2010b)) and Indian Ocean (WIND 28K) has been calculated over the last full glacial cycle (Fig. 5). This isolates ‘closed system’ processes such as ocean circulation, and biological redistribution of DIC and ALK within ocean basins. Differenced data were calculated by interpolating the high resolution WIND 28K record to measured VM28-122 age intervals; both age models are matched to the LR04 global benthic stack (Lisiecki and Raymo, 2005). Due to the shallow sill depth of the Caribbean Basin, site VM28-122 is thought to be recording an intermediate water mass signal (Yu et al., 2013), while WIND 28K is recording deep water changes in the Indian Ocean. $[\text{CO}_3^{2-}]$ and $\delta^{13}\text{C}$ gradients between VM28-122 and WIND 28K increase throughout glaciation, with particularly large gradients during MIS 2 and MIS 4, when atmospheric CO_2 reached a minima (Fig. 5). This is in agreement with the nutrient deepening hypothesis, which states that carbon is transferred from surface and intermediate waters to the deep ocean during glacial periods (Boyle, 1988). We suggest that changes in deep ocean carbon storage and associated carbonate compensation responses are driving transient changes in $[\text{CO}_3^{2-}]$ that are recorded at site WIND 28K. This idea is supported by a significant

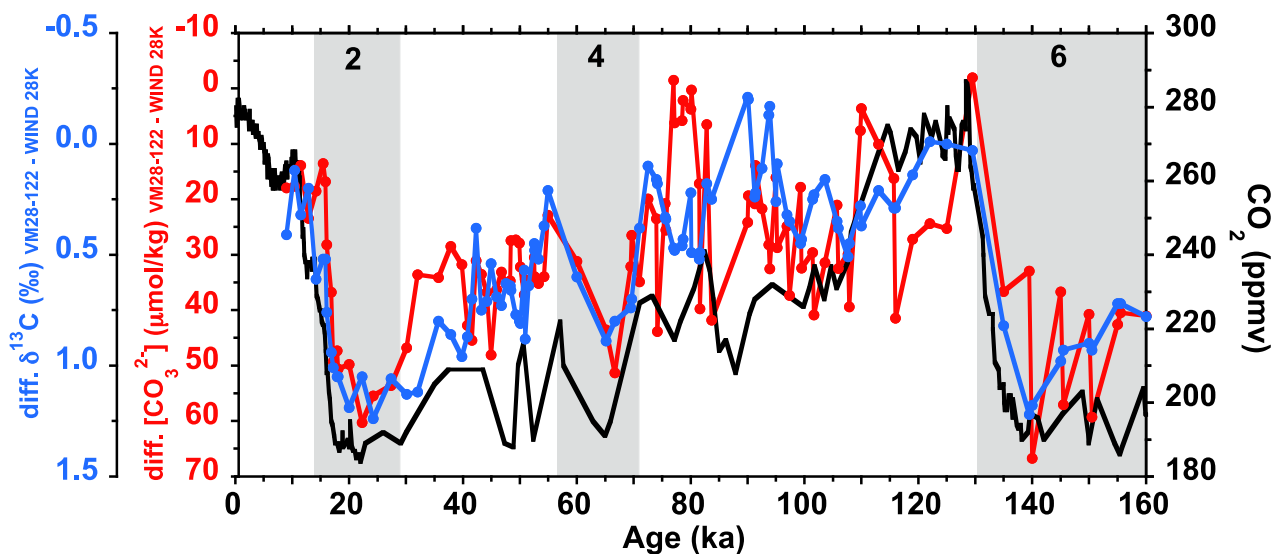


Figure 5: Difference between Caribbean Basin (VM28-122, Yu et al., 2010b) and Indian Ocean (WIND 28K) $[\text{CO}_3^{2-}]$ ($\mu\text{mol/kg}$) (red) and $\delta^{13}\text{C}$ (‰) (blue)). Data has been reversed to show agreement with atmospheric CO_2 (black). Grey bars show Marine Isotope Stages. Atmospheric CO_2 data are from Petit et al. (1999). $[\text{CO}_3^{2-}]$ data are from Yu et al. (2010b) (VM28-122), Yu et al. (2010a) (WIND 28K <47.85 ka). $\delta^{13}\text{C}$ data are from McCave et al. (2005) (WIND 28K), and Yu et al. (2010b) (VM28-122).

351 depletion of $\delta^{13}\text{C}_{(\text{atm})}$ during MIS 4, and enrichment of similar magnitude during the
352 transition into MIS 3 (Eggleston et al., 2016). There is no clear trend of change in the
353 $[\text{CO}_3^{2-}]$ gradient during MIS 5 (Fig. 5), further supporting our hypothesis that a whole ocean
354 increase in ALK from removal of shelf areas for CaCO_3 burial is driving a global increase in
355 $[\text{CO}_3^{2-}]$.

356

357 Rapid changes in deep ocean carbon storage during the time from MIS 5 to MIS 3 could be
358 driven by changes in ocean circulation and/or biological processes. The MIS 5 to MIS 4
359 transition marks a shift towards more southern-sourced waters in the deep Indian Ocean
360 (Piotrowski et al., 2009). This shift resulted from a shoaling of NADW influence to ~2-3 km
361 water depth in the Atlantic Ocean (Thornalley et al., 2015? SS paper). Shoaling of
362 NADW acted to increase deep ocean stratification and enhance carbon storage (Adkins,
363 2013). A more efficient Southern Ocean biological pump, driven by alleviation of iron
364 limitation, could have further increased the deep ocean pool of respired DIC (Martin and
365 Fitzwater, 1988).

366

367 Site ODP 806 records similar transient changes in $\delta^{13}\text{C}$ and $[\text{CO}_3^{2-}]$ over the past five
368 glacial cycles (Fig. 3B). Sampling resolution and sedimentation rate restrict our ability to
369 assess these in detail, however $[\text{CO}_3^{2-}]$ and $\delta^{13}\text{C}$ appear to be responding to increases in
370 deep ocean carbon storage in the same way as site WIND 28K, causing rapid reductions in
371 both $[\text{CO}_3^{2-}]$ and $\delta^{13}\text{C}$ that coincide with a decline in atmospheric $p\text{CO}_2$ (Fig. 3B) and result
372 in a deviation away from the longer term increasing trend (Fig. 2B). Site TT013-PC72 in the
373 central Pacific Ocean does not record any transient changes in $[\text{CO}_3^{2-}]$ away from the long-
374 term increasing trend (Fig. 3C). This may be an artifact of sampling resolution and/or the
375 low accumulation rate at this site, which at certain intervals is as low as 0.5 cm/ky.

376

377 **3.2.2 Deglacial carbon removal from the deep ocean**

378

379 In addition to transient declines in deep ocean $[\text{CO}_3^{2-}]$ that cause deviations away from the
380 longer-term increasing trend, WIND 28K records transient rises $[\text{CO}_3^{2-}]$ during deglaciation
381 (Fig. 2A). WIND 28K is the only record presented here with sufficient resolution to
382 accurately record these transient peaks (Fig. 2).

383 Between ~139 ka and ~129 ka, when atmospheric CO_2 rose by ~100 ppm, $[\text{CO}_3^{2-}]$ and

384 $\delta^{13}\text{C}$ increased by $\sim 10 \text{ } \mu\text{mol/kg}$ and $\sim 0.5\text{‰}$ respectively at site WIND 28K (Fig.3A).
385 Modeling work suggests that release of carbon stored in the deep ocean will cause such a
386 peak (Boyle, 1988) as removal of respired carbon stored causes a rapid rise in both $[\text{CO}_3^{2-}]$
387 and $\delta^{13}\text{C}$, which is followed by a reduction in $[\text{CO}_3^{2-}]$ as CaCO_3 burial acts to restore steady
388 state conditions (Fig. 3A). This CaCO_3 burial has little effect on $\delta^{13}\text{C}$, resulting in a
389 decoupled response of $\delta^{13}\text{C}$ and $[\text{CO}_3^{2-}]$.

390 The $\sim 10 \text{ } \mu\text{mol/kg}$ increase in $[\text{CO}_3^{2-}]$ at the MIS 6 to MIS 5 transition is remarkably similar
391 to the rise recorded at the same site during the last deglaciation (Yu et al., 2010a), implying
392 a robust carbonate system response to carbon removal. Yu et al. (2010a) estimate that if
393 deep waters recording a $\sim 10 \text{ } \mu\text{mol/kg}$ deglacial peak in $[\text{CO}_3^{2-}]$ represent 30% of the global
394 ocean volume, this can account for approximately half of the total atmospheric $p\text{CO}_2$ rise.
395 Sites ODP 806 and TT013-PC72 do not have sufficiently high sampling resolution to
396 accurately resolve these deglacial peaks and confirm the presence of a deglacial $[\text{CO}_3^{2-}]$
397 rise in the Pacific Ocean (Fig. 3). However, Yu et al. (2010a) did resolve a deglacial peak
398 during last deglaciation at TTN013-PC61 in the deep Central Equatorial Ocean. This site
399 records a similar magnitude of increase at the last deglaciation as WIND 28K, and almost
400 identical $[\text{CO}_3^{2-}]$ trends to TT013-PC72 (Yu et al., 2013). As a result, it is reasonable to
401 assume that the penultimate deglacial peak recorded in the deep Indian Ocean is also
402 representative of the deep Pacific Ocean, however further high resolution records in the
403 deep Pacific Ocean are required to confirm this.

404 **3.3 Magnitude of glacial $[\text{CO}_3^{2-}]$ increase**

405 As we have shown, transient shifts in $[\text{CO}_3^{2-}]$ driven by changes in carbon storage are met
406 with carbonate compensation processes that act to restore steady state conditions. This
407 buffering nature of the carbonate system makes it difficult to constrain the magnitude of
408 ALK increase. Furthermore, deep ocean $[\text{CO}_3^{2-}]$ is controlled by both ALK and DIC, thus
409 estimating deep ocean ALK from $[\text{CO}_3^{2-}]$ requires assumptions regarding the processes
410 that are driving the $[\text{CO}_3^{2-}]$ change. For example, an increase in $[\text{CO}_3^{2-}]$ that is caused by
411 dissolution of seafloor CaCO_3 or removal of shelf area for CaCO_3 deposition constitutes an
412 ALK increase that could drive carbon sequestration. However an increase in $[\text{CO}_3^{2-}]$ that is
413 driven by carbon removal does not represent an increase in whole ocean ALK and will not
414 increase carbon storage. This means that there is no simple relationship between changes

415 in deep water $[\text{CO}_3^{2-}]$ and ALK. As a result, we are restricted to estimating the $[\text{CO}_3^{2-}]$
 416 increase that is likely driven by a rise in whole ocean ALK, and cannot directly measure the
 417 magnitude of ALK rise from $[\text{CO}_3^{2-}]$ alone.

418 The complex nature of estimating the glacial increase in $[\text{CO}_3^{2-}]$ that is driven by a rise in
 419 whole ocean ALK is exemplified in Figure 6. Rickaby et al. (2010) and Yu et al. (2013)
 420 measured $[\text{CO}_3^{2-}]$ changes in the Weddell Sea and Pacific Ocean, respectively. Both
 421 records show a long-term glacial $[\text{CO}_3^{2-}]$ increase during the last glaciation, but they report
 422 very different magnitudes of $[\text{CO}_3^{2-}]$ change of $\sim 25 \mu\text{mol/kg}$ (Rickaby et al., 2010) versus
 423 $\sim 7 \mu\text{mol/kg}$ (Yu et al., 2013). There is good agreement in the magnitude of $\Delta[\text{CO}_3^{2-}]$
 424 changes at TT013-PC72 (this study), the Weddell Sea (PS1506) (Rickaby et al., 2010) and
 425 Pacific Ocean (MW91-9-GGC48) (Yu et al., 2013) (Fig. 6). We suggest that quantification of
 426 the glacial $[\text{CO}_3^{2-}]$ increase by Rickaby et al. (2010) was likely overestimated as a result of
 427 low sampling resolution and resultant sampling of deglacial peaks that are driven by
 428 removal of carbon from the deep ocean, rather than in increase in ocean ALK that may act
 429 to lower atmospheric $p\text{CO}_2$.

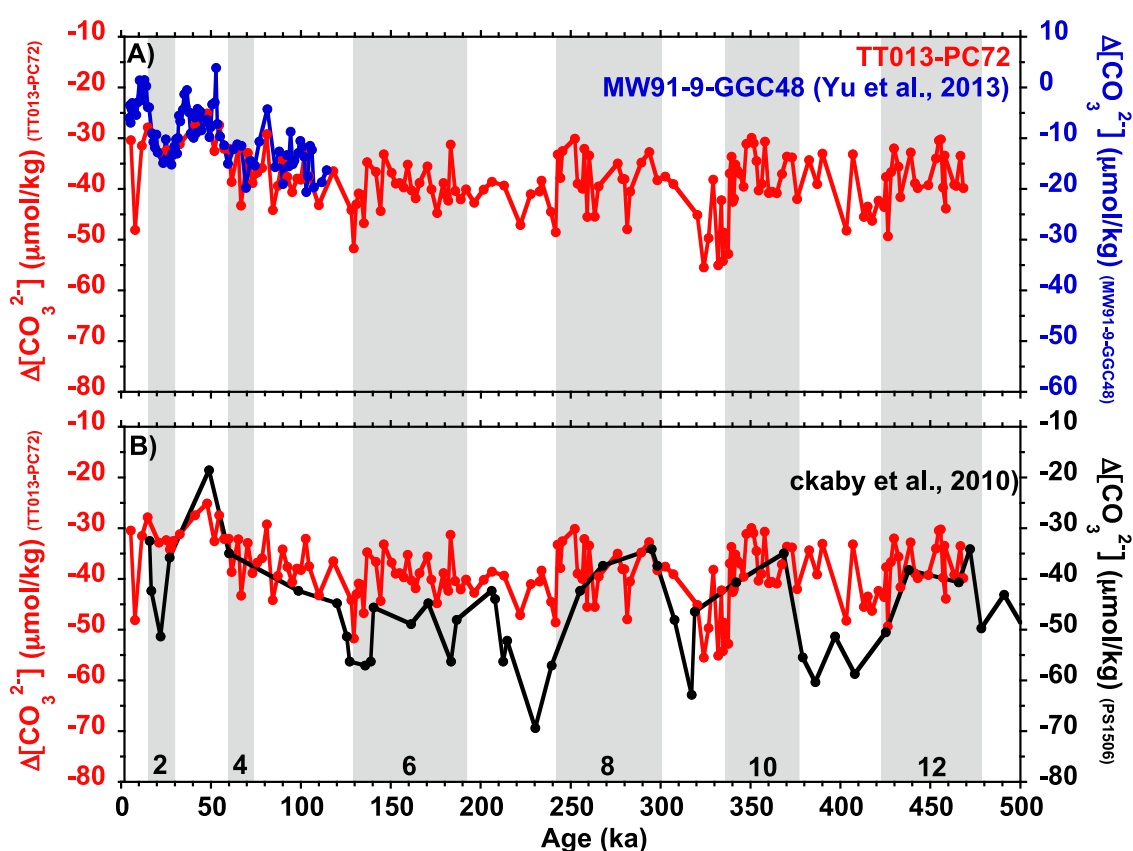


Figure 6: Glacial-interglacial change in $\Delta[\text{CO}_3^{2-}]$ ($\mu\text{mol/kg}$) at A) TT013-PC72 (red) and MW91-9-GGC48 (blue), and B) TT013-PC72 (red) and PS1506 (black). Grey bars show Marine Isotope Stages. Data are from this study (TT013-PC72), Rickaby et al. (2010) (PS1506) and Yu et al. (2013a) (MW91-9-GGC48).

440 As previously mentioned, the high sampling resolution of WIND 28K highlights transient
441 responses that are not identifiable at sites TT013-PC72 or ODP 806. Published records
442 from proximate locations in the deep Pacific Ocean (Yu et al., 2013, 2010a) indicate that
443 these processes are recorded, and their absence from the records shown is likely an
444 artifact of sampling resolution. As a result, estimations of long-term changes TT013-PC72
445 and ODP 806 locations may be overestimated.

446 In the deep Indian Ocean (WIND 28K) there is a glacial increase in $[\text{CO}_3^{2-}]$ of $\sim 7.4 \mu\text{mol/kg}$
447 over the last full glacial cycle. This increase is calculated as the difference between the
448 averages of all data points from 123-115 ka and from 23-19 ka. Minimal $[\text{CO}_3^{2-}]$ interglacial
449 conditions are measured at between 115 ka and 123 ka as the burial of CaCO_3 on shelves
450 and in the deep sea is driving a reduction in $[\text{CO}_3^{2-}]$ prior to this (Fig. 3A). To reduce the
451 influence of these transient changes on the estimation of the glacial $[\text{CO}_3^{2-}]$ rise in the lower
452 resolution records (ODP 806 and TT013-PC72) we have calculated a 10 ky moving
453 average (Fig. 2D). Based on the smoothed record, the glacial increase in ocean $[\text{CO}_3^{2-}]$
454 estimated at site TT013-PC72 ranges from $6.0 \mu\text{mol/kg}$ (MIS 7 to MIS 6) to $10.8 \mu\text{mol/kg}$
455 (MIS 5 to MIS 2, and MIS 11 to MIS 10). Considering the analytical uncertainty (± 5.71
456 $\mu\text{mol/kg}$, 2σ), there seems to be no significant difference in the magnitude of glacial $[\text{CO}_3^{2-}]$
457 increase over the last four glacial cycles at site TT013-PC72. The average glacial increase
458 in $[\text{CO}_3^{2-}]$ over the last four glacial cycles at this site is 9.2 ± 4.5 (2σ) $\mu\text{mol/kg}$.

459 Site ODP 806 records a much larger range in the magnitude of $[\text{CO}_3^{2-}]$ rise over the past
460 five glacial cycles. $[\text{CO}_3^{2-}]$ increased by $16.1 \mu\text{mol/kg}$ from 124 ka to 24 ka (MIS 5 to MIS
461 2), while no clear increase is recorded from MIS 13 to MIS 12 (Fig. 2B). Another obvious
462 feature is the low $[\text{CO}_3^{2-}]$ during MIS 10, which may be at least partially affected by
463 bioturbation because benthic $\delta^{18}\text{O}$ did not increase as much as expected based on the
464 LR04 curve (Lisiecki and Raymo, 2005) (Supplementary Material 4). We estimate that the
465 $[\text{CO}_3^{2-}]$ increase recorded at site ODP 806 over each of the last five glacial cycles is $7.3 \pm$
466 11.8 (2σ) $\mu\text{mol/kg}$. The variability at this site is likely caused by the low sampling resolution
467 (~ 5 ky), which limits the effectiveness of the 10-ky smoothed record to reduce the influence
468 of transient $[\text{CO}_3^{2-}]$ changes on the longer-term trend. Intermittent sampling of these
469 transient changes could have amplified this effect.

470 Sites WIND 28K and TT013-PC72 provide a more accurate measure of the glacial $[\text{CO}_3^{2-}]$

rise. The higher sampling resolution at site WIND 28K (~0.6 ky) permits elimination of transient changes that are not indicative of the longer-term trend, while TT013-PC72 does not record a transient decline in $[\text{CO}_3^{2-}]$ as carbon is transferred to the deep ocean (see Section 3.2.1) and the sampling resolution (~3 ky) is sufficient to reduce the effect of transient increases on the glacial rise in the smoothed record (Fig. 2D). Our estimate of the increase in glacial ocean $[\text{CO}_3^{2-}]$ recorded at site TT013-PC72 of 9.2 ± 4.5 (2σ) $\mu\text{mol/kg}$ is similar to that based on WIND 28K from the deep Indian Ocean over the last full glacial cycle (7.4 $\mu\text{mol/kg}$). Coherent changes, observed in cores from disparate locations (WIND 28K and TT013-PC72), suggest that a carbon-rich and high ALK water mass bathed a large proportion of the glacial deep ocean during the last glaciation. This recorded glacial $[\text{CO}_3^{2-}]$ increase likely represents an underestimation of the global increase in ocean ALK, due to a simultaneous increase in the deep ocean DIC content driving a reduction in $[\text{CO}_3^{2-}]$.

4. Conclusions

Glacial-interglacial changes in deep Indian and Pacific Ocean $[\text{CO}_3^{2-}]$ are mainly controlled by two mechanisms that operate on different timescales: 1) a long-term glacial increase driven by a reduction in sea level and shift of ALK from shelf areas to the deep ocean, and 2) transient carbonate compensation responses to changes in deep ocean carbon storage.

Transient shifts in $[\text{CO}_3^{2-}]$ and $\delta^{13}\text{C}$ are indicative of changes in the degree of carbon storage by transfer of carbon from the upper ocean to the deep ocean, and vice versa. These transient changes cause deviation of $[\text{CO}_3^{2-}]$ away from the long-term trend, showing negative $[\text{CO}_3^{2-}]$ excursions as carbon enters the deep ocean and $[\text{CO}_3^{2-}]$ peaks as carbon is transferred to the upper ocean and atmosphere.

Arguably the most important feature of the records shown is the long-term glacial increase. This is a robust feature of the last five glacial cycles in the deep Pacific Ocean (4.3 km). We suggest that the inferred increase in ocean ALK is driven by a drop in glacial sea level and associated decrease in neritic CaCO_3 deposition on shelf areas. This increase in whole ocean ALK could act to drive a reduction in atmospheric $p\text{CO}_2$ before any major change in water mass organization.

Accurate constraint of the magnitude of the glacial ALK increase is beyond the scope of this study. We have shown that deep ocean $[\text{CO}_3^{2-}]$ is driven by both DIC and ALK on glacial-

interglacial timescales, therefore $[\text{CO}_3^{2-}]$ shifts are not necessarily representative of changes in whole ocean ALK. In order to estimate changes in the whole ocean ALK budget from $[\text{CO}_3^{2-}]$ reconstructions we must first understand the processes that are driving the changes. Importantly, this implies that time slice comparisons (i.e. Holocene and LGM) may not be a suitable approach to estimate whole ocean changes in ALK from $[\text{CO}_3^{2-}]$.

We estimate that glacial deep Pacific Ocean $[\text{CO}_3^{2-}]$ increased by 9.2 ± 4.5 (2σ) $\mu\text{mol/kg}$ over each glaciation of the last 500 ka. This increase is representative of the $[\text{CO}_3^{2-}]$ rise recorded in the deep Indian Ocean over the last full glacial cycle ($7.4 \mu\text{mol/kg}$). We have attempted to eliminate $[\text{CO}_3^{2-}]$ changes that are driven by carbon removal during deglaciation, therefore although we are unable to accurately constrain the magnitude of glacial ALK increase, we suggest that this $[\text{CO}_3^{2-}]$ rise is driven by an increase in whole ocean ALK. Agreement between the magnitude of change recorded at such disparate locations indicates that a carbon rich, high ALK, water mass bathed a large proportion of the glacial deep ocean during the last glaciation. Furthermore, there is no significant difference in glacial $[\text{CO}_3^{2-}]$ rise recorded during each of the last four glaciations in the deep Pacific Ocean (4.3 km). Consequently, the inferred glacial increase in whole ocean ALK from redistribution of shelf CaCO_3 to the deep-ocean, is a robust mechanism that may have played a key role in driving carbon sequestration before major water mass reorganization. We urge future studies to generate more detailed reconstructions at high sedimentation sites in the deep Pacific, which are critical to improve our understanding about past atmospheric pCO_2 changes.

Acknowledgements

This work was funded by The European Research Council (ERC grant 2010- NEWLOG ADG-267931 to HE), and Australian Research Council (DP140101393 and FT140100993 to JY). We would like to thank Prof. Robert Anderson for donation of TT013-PC72 sediment samples and valuable discussion, and Prof. Alan Mix for allowing us to use his unpublished benthic $\delta^{13}\text{C}$ record from site TT013-PC72.

References

Adkins, J.F., 2013. The role of deep ocean circulation in setting glacial climates.

534 Paleoceanography 28, 539–561. doi:10.1002/palo.20046

535 Anderson, R.F., Fleisher, M.Q., Lao, Y., Winckler, G., 2008. Modern CaCO₃ preservation in
 536 equatorial Pacific sediments in the context of late-Pleistocene glacial cycles. *Mar.*
 537 *Chem.* 111, 30–46. doi:10.1016/j.marchem.2007.11.011

538 Archer, D., Maier-Reimer, E., 1994. Effect of deep-sea sedimentary calcite preservation on
 539 atmospheric CO₂ concentration. *Nature* 367, 260–263. doi:10.1038/367260a0

540 Barker, S., Greaves, M., Elderfield, H., 2003. A study of cleaning procedures used for
 541 foraminiferal Mg/Ca paleothermometry. *Geochemistry Geophys. Geosystems* 4, 1–20.
 542 doi:10.1029/2003GC000559

543 Berger, W.H., 1982. Increase of carbon dioxide in the atmosphere during deglaciation: the
 544 coral reef hypothesis. *Naturwissenschaften* 69, 87–88. doi:10.1007/BF00441228

545 Bickert, T., Berger, H., Burke, S., Schmidt, H., Wefer, G., 1993. Late Quaternary Stable
 546 Isotope Record of Benthic Foraminifers: Site 805 and 806, Ontong Java Plateau. *Proc.*
 547 *Ocean Drill. Program, Sci. Results* 411–420.

548 Boyle, E.A., 1988. The role of vertical chemical fractionation in controlling late Quaternary
 549 atmospheric carbon dioxide. *J. Geophys. Res.* 93, 15701–15714.
 550 doi:10.1029/JC093iC12p15701

551 Broecker, W.S., Peng, T.-H., 1989. The cause of the glacial to interglacial atmospheric CO₂
 552 change: A Polar Alkalinity Hypothesis. *Global Biogeochem. Cycles* 3, 215–239.
 553 doi:10.1029/GB003i003p00215

554 Broecker, W.S., Sutherland, S., 2000. Distribution of carbonate ion in the deep ocean:
 555 Support for a post-Little Ice Age change in Southern Ocean ventilation? *Geochemistry,*
 556 *Geophys. Geosystems* 1, 1023. doi:10.1029/2000GC000039

557 Catubig, N.R., Archer, D.E., Francois, R., DeMenocal, P., Howard, W., Yu, E., 1998. Global
 558 deep-sea burial rate of calcium carbonate during the Last Glacial Maximum.
 559 *Paleoceanography* 13, 298–310. doi:10.1029/98PA00609

560 Dickson, A.G., 1990. Thermodynamics of the dissociation of boric acid in synthetic
 561 seawater from 273 . 15 to 318 . 15 K 37, 755–766. doi:10.1016/0198-0149(90)90004-F

562 Dickson, A.G., Millero, F.J., 1987. A comparison of the equilibrium constants for the
 563 dissociation of carbonic acid in seawater media. *Deep Sea Res. Part A. Oceanogr.*
 564 *Res. Pap.* 34, 1733–1743. doi:10.1016/0198-0149(87)90021-5

565 Eggleston, S., Schmitt, J., Bereiter, B., Schneider, R., Fischer, H., 2016. Evolution of the
 566 stable carbon isotope composition of atmospheric CO₂ over the last glacial cycle.
 567 *Paleoceanography* 31. doi:10.1002/2015PA002874

568 Foster, G.L., Vance, D., 2006. Negligible glacial-interglacial variation in continental
 569 chemical weathering rates. *Nature* 444, 918–921. doi:10.1038/nature05365

570 Gibbs, M.T., Kump, L.R., 1994. Global chemical erosion during the Last Glacial Maximum
 571 and the present: Sensitivity to changes in lithology and hydrology. *Paleoceanography*
 572 9, 529–543. doi:10.1029/94PA01009

573 Grant, K.M., Rohling, E.J., Bar-Matthews, M., Ayalon, A., Medina-Elizalde, M., Ramsey,
 574 C.B., Satow, C., Roberts, A.P., 2012. Rapid coupling between ice volume and polar
 575 temperature over the past 150000 years. *Nature* 491, 744–747.

doi:10.1038/nature11593

Grant, K.M., Rohling, E.J., Ramsey, C.B., Cheng, H., Edwards, R.L., Florindo, F., Heslop, D., Marra, F., Roberts, A.P., Tamisiea, M.E., Williams, F., 2014. Sea-level variability over five glacial cycles. *Nat. Commun.* 5, 5076. doi:10.1038/ncomms6076

Janecek, T.R., 1993. Data Report: High-resolution carbonate and bulk grain size data for sites 803-806 (0-2MA). *Proc. Ocean Drill. Program, Sci. Results* 130, 761–773.

Johnstone, H.J.H., Kiefer, T., Elderfield, H., Schulz, M., 2014. Calcite saturation, foraminiferal test mass, and Mg/Ca-based temperatures dissolution corrected using XDX-A 150 ka record from the western Indian Ocean. *Geochemistry Geophys. Geosystems* 15, 781–797. doi:10.1002/2013GC004994

Key, R.M., Kozyr, A., Sabine, C.L., Lee, K., Wanninkhof, R., Bullister, J.L., Feely, R.A., Millero, F.J., Mordy, C., Peng, T.H., 2004. A global ocean carbon climatology: Results from Global Data Analysis Project (GLODAP). *Global Biogeochem. Cycles* 18. doi:10.1029/2004GB002247

Lisiecki, L.E., Raymo, M.E., 2005. A Pliocene-Pleistocene stack of 57 globally distributed benthic $\delta^{18}\text{O}$ records. *Paleoceanography* 20. doi:10.1029/2004PA001071

Lüthi, D., Le Floch, M., Bereiter, B., Blunier, T., Barnola, J.-M., Siegenthaler, U., Raynaud, D., Jouzel, J., Fischer, H., Kawamura, K., Stocker, T.F., 2008. High-resolution carbon dioxide concentration record 650,000-800,000 years before present. *Nature* 453, 379–382. doi:10.1038/nature06949

Martin, J.H., Fitzwater, S.E., 1988. Iron deficiency limits phytoplankton growth in the north-east Pacific subarctic. *Nature* 331, 947–975. doi:10.1038/331341a0

McCave, I.N., Kiefer, T., Thornalley, D.J.R., Elderfield, H., 2005. Deep flow in the Madagascar-Mascarene Basin over the last 150,000 years. *Philos. Trans. A. Math. Phys. Eng. Sci.* 363, 81–99. doi:10.1098/rsta.2004.1480

Mehrbach, C., 1973. Measurement of the apparent dissociation constants of carbonic acid in seawater at atmospheric pressure. *Limnol. Oceanogr.* 18, 897–907.

Milliman, J.D., 1993. Production and accumulation of calcium carbonate in the ocean: Budget of a nonsteady state. *Global Biogeochem. Cycles* 7, 927–957. doi:10.1029/93GB02524

Milliman, J.D., Müller, G., Förstner, U., 1974. *Recent Sedimentary Carbonates: Part 1 - Marine Carbonates*. Springer Berlin Heidelberg. doi:10.1007/978-3-642-65528-9

Misra, S., Greaves, M., Owen, R., Kerr, J., Elmore, A.C., Elderfield, H., 2014. Determination of B/Ca of natural carbonates by HR-ICP-MS. *Geochemistry, Geophys. Geosystems* 15, 1617–1628. doi:10.1002/2013GC005049

Monnin, E., Indermühle, A., Dällenbach, A., Flückiger, J., Stauffer, B., Stocker, T.F., Raynaud, D., Barnola, J.M., 2001. Atmospheric CO₂ concentrations over the last glacial termination. *Science* 291, 112–114. doi:10.1126/science.291.5501.112

Munhoven, G., 2002. Glacial–interglacial changes of continental weathering: estimates of the related CO₂ and HCO₃[−] flux variations and their uncertainties. *Glob. Planet. Change* 33, 155–176. doi:10.1016/S0921-8181(02)00068-1

Opdyke, B.N., Walker, J.C.G., 1992. Return of the coral reef hypothesis: Basin to shelf

618 partitioning of CaCO₃ and its effect on atmospheric CO₂. *Geology* 20, 733–736.
619 doi:10.1130/0091-7613(1992)020

620 Pelletier, G., Lewis, E., Wallace, D., 2005. A calculator for the CO₂ system in seawater for
621 Microsoft Excel/VBA.

622 Petit, J.R., Raynaud, D., Basile, I., Chappellaz, J., Ritz, C., Delmotte, M., Legrand, M.,
623 Lorius, C., Pe, L., 1999. Climate and atmospheric history of the past 420,000 years
624 from the Vostok ice core, Antarctica. *Nature* 399, 429–436.

625 Piotrowski, A.M., Banakar, V.K., Scrivner, A.E., Elderfield, H., Galy, A., Dennis, A., 2009.
626 Indian Ocean circulation and productivity during the last glacial cycle. *Earth Planet. Sci.*
627 *Lett.* 285, 179–189. doi:10.1016/j.epsl.2009.06.007

628 Rickaby, R.E.M., Elderfield, H., Roberts, N., Hillenbrand, C.D., Mackensen, A., 2010.
629 Evidence for elevated alkalinity in the glacial Southern Ocean. *Paleoceanography* 25,
630 1–15. doi:10.1029/2009PA001762

631 Ridgwell, A., Hargreaves, J.C., 2007. Regulation of atmospheric CO₂ by deep-sea
632 sediments in an Earth system model. *Global Biogeochem. Cycles* 21, GB002764.
633 doi:10.1029/2006GB002764

634 Siegenthaler, U., Stocker, T.F., Monnin, E., Lüthi, D., Schwander, J., Stauffer, B., Raynaud,
635 D., Barnola, J.-M., Fischer, H., Masson-Delmotte, V., Jouzel, J., 2005. Stable carbon
636 cycle-climate relationship during the Late Pleistocene. *Science* 310, 1313–1317.
637 doi:10.1126/science.1120130

638 Toole, J.M., Warren, B.A., 1993. A hydrographic section across the subtropical South
639 Indian Ocean. *Deep Sea Res. Part I Oceanogr. Res. Pap.* 40, 1973–2019.
640 doi:10.1016/0967-0637(93)90042-2

641 Uppström, L.R., 1974. The boron/chlorinity ratio of deep-sea water from the Pacific Ocean.
642 *Deep Sea Res. Oceanogr. Abstr.* 21, 161–162. doi:10.1016/0011-7471(74)90074-6

643 Wallmann, K., Schneider, B., Sarnthein, M., 2016. Effects of eustatic sea-level change,
644 ocean dynamics, and iron fertilization on atmospheric pCO₂ and seawater composition
645 over the last 130 000 years: a model study. *Clim. Past* 12, 339–375. doi:10.5194/cp-
646 12-339-2016

647 Winckler, G., Anderson, R.F., Fleisher, M.Q., McGee, D., Mahowald, N., 2008. Covariant
648 glacial-interglacial dust fluxes in the equatorial Pacific and Antarctica. *Science* 320, 93–
649 96. doi:10.1126/science.1150595

650 Yu, J., Anderson, R.F., Jin, Z., Rae, J.W.B., Opdyke, B.N., Eggins, S.M., 2013. Responses
651 of the deep ocean carbonate system to carbon reorganization during the Last Glacial–
652 interglacial cycle. *Quat. Sci. Rev.* 76, 39–52. doi:10.1016/j.quascirev.2013.06.020

653 Yu, J., Broecker, W.S., Elderfield, H., Jin, Z., McManus, J., Zhang, F., 2010a. Loss of
654 carbon from the deep sea since the Last Glacial Maximum. *Science* 330, 1084–1087.
655 doi:10.1126/science.1193221

656 Yu, J., Day, J., Greaves, M., Elderfield, H., 2005. Determination of multiple element/calcium
657 ratios in foraminiferal calcite by quadrupole ICP-MS. *Geochemistry, Geophys.*
658 *Geosystems* 6, GC000964. doi:10.1029/2005GC000964

659 Yu, J., Elderfield, H., 2007. Benthic foraminiferal B/Ca ratios reflect deep water carbonate
660 saturation state. *Earth Planet. Sci. Lett.* 258, 73–86. doi:10.1016/j.epsl.2007.03.025

- Yu, J., Elderfield, H., Piotrowski, A.M., 2008. Seawater carbonate ion $\delta^{13}\text{C}$ systematics and application to glacial–interglacial North Atlantic ocean circulation. *Earth Planet. Sci. Lett.* 271, 209–220. doi:10.1016/j.epsl.2008.04.010
- Yu, J., Foster, G.L., Elderfield, H., Broecker, W.S., Clark, E., 2010b. An evaluation of benthic foraminiferal B/Ca and d^{11}B for deep ocean carbonate ion and pH reconstructions. *Earth Planet. Sci. Lett.* 293, 114–120. doi:10.1016/j.epsl.2010.02.029
- Yu, J., Menviel, L., Jin, Z.D., Thornalley, D.J.R., Barker, S., Marino, G., Rohling, E.J., Cai, Y., Zhang, F., Wang, X., Dai, Y., Chen, P., Broecker, W.S., 2016. Sequestration of carbon in the deep Atlantic during the last glaciation. *Nat. Geosci.* doi:10.1038/ngeo2657

697
698
699
700

701 Supplementary material

702 Supplementary material 1

703 Size fraction effect on the B/Ca of *C. wuellerstorfi* shells

704 There is large variation in the size fraction of individual *C. wuellerstorfi* shells, from <150 μm
705 to >500 μm . To ensure that there is no consistent size fraction effect on B/Ca ratios, *C.*
706 *wuellerstorfi* samples were split into size fractions (~8 shells each) and analysed separately
707 using HR-ICP-MS (see Supplement 2 for method details). There is no consistent offset
708 between B/Ca ratios measured in different size fractions of *C. wuellerstorfi* (Fig. S1). *C.*
709 *wuellerstorfi* shells of all size fractions (180-500 μm) were used in this study.

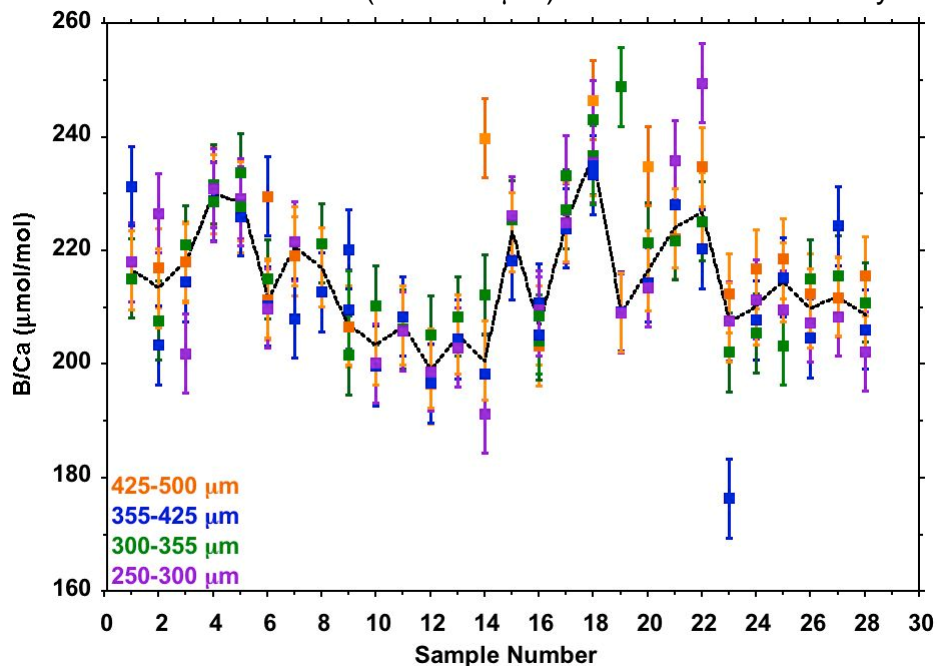


Figure S1: B/Ca ($\mu\text{mol/mol}$) in different size fractions of *C. wuellerstorfi* shells. 425-500 μm (orange), 355-425 μm (blue), 300-355 μm (green), and 250-300 μm (purple). The average of all size fractions is in black. Error = 7.0 $\mu\text{mol/mol}$, (2σ) from repeat analysis of a laboratory standard with a concentration of 198.6 $\mu\text{mol/mol}$ ($n = 144$).

721

722

723

724

725 **Supplementary material 2**

726 **Sample preparation and trace element determination**

727 Sediment samples of $\sim 10 \text{ cm}^3$, from 2 cm segments, were disaggregated in deionized
728 water and wet sieved through $63 \mu\text{m}$ sieves. A small quantity of sediment ($\sim 0.5 \text{ cm}^3$) was
729 removed prior to wet sieving for weight per cent CaCO_3 determination. Pristine *C.*
730 *wuellerstorfi* tests were picked from the $180\text{-}500 \mu\text{m}$ size fraction. Where foraminifera were
731 abundant, 10-15 shells were picked from the $250\text{-}500 \mu\text{m}$ size fraction ($0.3\text{-}0.5 \text{ mg}$),
732 however where benthic foraminifera were sparse preference was given to fewer shells
733 (minimum of 3) with consistent morphology (Rae et al., 2011). Picked shells were gently
734 crushed between glass plates, split for stable isotope determination, and cleaned according
735 the oxidative, "Mg/Ca-cleaning" protocol outlined in Barker et al. (2003).

736

737 Sediment weight per cent CaCO_3 was determined by acidifying dried bulk sediment with
738 10% phosphoric acid and measuring the CO_2 released using a UIC 5011 CO_2 coulometer.
739 Analytical precision by replicate analysis of a carbonate standard was 2.05% (2σ , $n = 60$).
740 Stable isotope determination was carried out at the Godwin Laboratory, University of
741 Cambridge, using a VG SIRA mass spectrometer, and for mass limited samples, a
742 Thermo® Kiel device connected to a Thermo® MAT 253 isotope ratio mass spectrometer.
743 Results are reported with reference to the international standard VPDB and the long-term
744 instrumental precision is $\leq \pm 0.16\text{‰}$ (2σ) for $\delta^{18}\text{O}$ and $\leq \pm 0.12\text{‰}$ (2σ) for $\delta^{13}\text{C}$.

745

746 Trace element ratios of cleaned foraminifera shells were determined by Quadrupole ICP-
747 MS or Thermo® Element XR HR-ICP-MS at the University of Cambridge according to Yu et
748 al., (2005) and Misra et al., (2014), respectively. The method of Misra et al., (2014) was
749 used in preference as it permits accurate measurement of low mass samples, repeat
750 analysis, and reduced boron memory effects. However, much of the data presented here
751 were measured by Quadrupole ICP-MS before the development of the HR-ICP-MS method
752 of Misra et al., (2014). B/Ca measured by replicate analysis of an in house standard
753 solution is consistent between the two methods: $\text{B/Ca} = 153.29 \pm 7.56 \mu\text{mol/mol}$ (2σ $n = 88$)

and $154.88 \pm 6.26 \text{ } \mu\text{mol/mol}$ (2σ , $n = 8$) by Quadrupole ICP-MS and HR-ICP-MS respectively, therefore no identification of the method used for individual samples is given.

B/Ca was plotted against contaminant concentrations (Fe/Ca, Al/Ca, and Mn/Ca), a linear regression fitted, and R^2 values used to check for covariance as an indicator of contamination effects on trace element ratios. The maximum Mn/Ca concentration ranged from 0.46 to 0.57 mmol/mol and showed little correlation with B/Ca ($R^2 = 0.01$ to 0.27).

777

778 **Supplementary material 3**779 **Disagreement between internal laboratory standards and adjustment of linear**
780 **relationship of B/Ca and $\Delta[\text{CO}_3^{2-}]$**

781 Allen et al., (2012), and Coadic et al., (2013) remark that B/Ca ratios measured at the
 782 University of Cambridge are ~7% lower compared to Rutgers University and LSCE,
 783 respectively. A similar difference was measured for in house consistency standards when
 784 measured using different sets of calibration standards - these will be referred to as '2005'
 785 and '2011' standards. Both sets of calibration standards were used to determine B/Ca
 786 shown in this paper, therefore, investigation into the exact difference was carried out. In
 787 addition, '2005' standards were used for the B/Ca to $\Delta[\text{CO}_3^{2-}]$ calibration presented in Yu &
 788 Elderfield (2007), therefore adjustment to this relationship is required.

789

790 B/Ca concentrations measured in five standards ranging from ~20 to 200 $\mu\text{mol/mol}$ were
 791 consistently higher by an average of 9.4% when calculated using '2011' compared to '2005'
 792 calibration standards (Fig. S2). Both sets of calibration standards were run back to back
 793 during the same instrumental analysis to eliminate differences in instrumental drift.

794

795

796

797

798

799

800

801

802

803

804

805

806

807

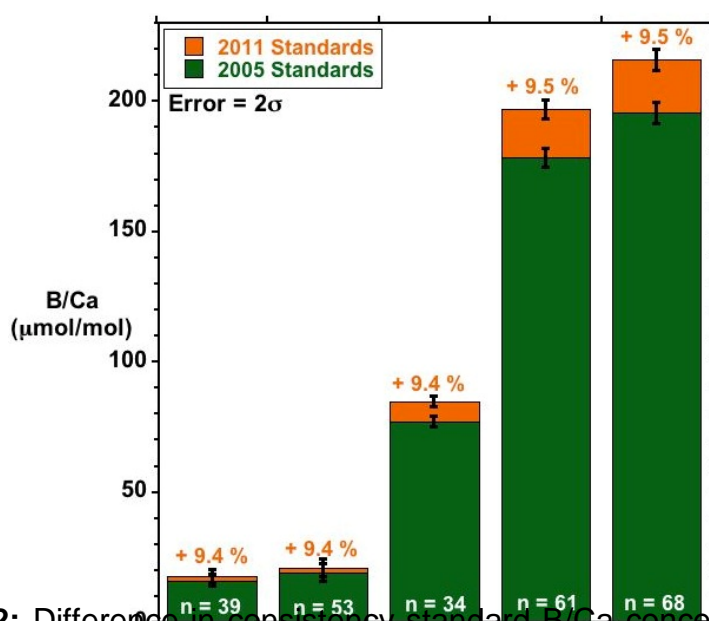


Figure S2: Difference in consistency standard B/Ca concentration ($\mu\text{mol/mol}$) when calculated using '2005' (green) and '2011' (orange) calibration standards. (A) '2011' Standard 1, (B) CAM-Uvig-2, (C) CAM-Mix, (D) CAM-wuellerstorfi, and (E) JCT-1 respectively. Error bars of 2σ are given on 34-68 analyses of each consistency standard.

808
809
810
811
812
813
814
815
816
817
818
819
820
821
822
823
824
825
826
827
828
829
830
831
832
833
834
835
836
837
838
839
840

The reason for this difference in B/Ca ratio when measured using '2005' and '2011' standards is currently unknown. Nevertheless, all B/Ca ratios measured using '2005' calibration standards shown in this paper have been increased by 9.4% to allow records measured using both sets of calibration standards to be combined and improve agreement with Rutgers and LSCE laboratories. All B/Ca data shown from Yu et al., (2013) and Yu et al., (2010) have also been adjusted to account for this difference.

An extensive core top calibration study by Yu & Elderfield (2007) showed that there is a significant, empirical relationship between B/Ca ratios in benthic foraminifera and deep ocean $\Delta[\text{CO}_3^{2-}]$. Data presented in Yu & Elderfield (2007) were analysed at the University of Cambridge using '2005' standards, therefore, an adjustment is required for all B/Ca ratios in Yu & Elderfield (2007) to bring them in line with samples measured using '2011' standards. An increase in all B/Ca measurements recorded by Yu & Elderfield (2007) by 9.4% changes the linear sensitivity of B/Ca ($\mu\text{mol/mol}$) to $\Delta[\text{CO}_3^{2-}]$ ($\mu\text{mol/kg}$) to:

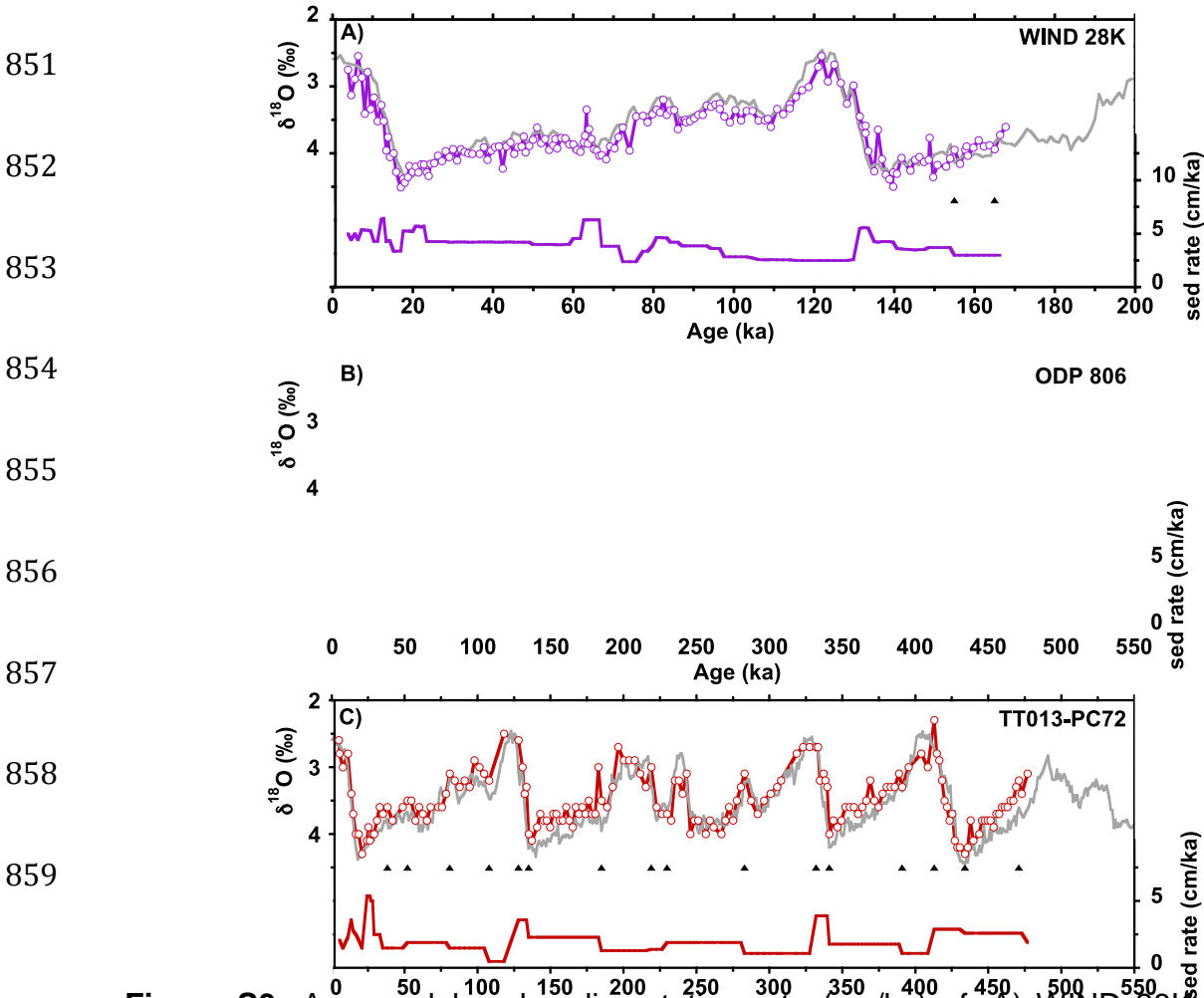
$$\Delta[\text{CO}_3^{2-}] = (\text{B/Ca} - 193) / 1.25, r^2 = 0.84, n = 176$$

Importantly, this change in sensitivity has a minimal effect on the calculated $[\text{CO}_3^{2-}]$, which remains well within instrumental uncertainty of $5.71 \mu\text{mol/kg}$ (2σ).

841

842 **Supplementary material 4 – Age models**

843 The age model of Medina-Elizalde and Lea (2005) was re-aligned to improve the fit with the
844 LR04 global benthic $\delta^{18}\text{O}$ stack (Lisiecki and Raymo, 2005) for ODP 806, using the $\delta^{18}\text{O}$ of
845 *C. wuellerstorfi*. The same approach was used at TT013-PC72 using the original age model
846 of Murray et al., (1995). Radiocarbon dates from Anderson et al., (2008) were used without
847 adjustment at <100 cm depth at TT013-PC72. The age model of Johnstone et al., (2014)
848 has been extended for WIND 28K, and the Yu et al., (2010) age model was used at <200
849 cm depth. Tie points were identified and linear interpolation applied between these tie
850 points. (Fig S3).



858 **Figure S3:** Age model and sedimentation rate (cm/ka) of: A) WIND 28K, B) ODP
859 806, and C) TT013-PC72. LR04 $\delta^{18}\text{O}$ stack is shown by grey lines (Lisiecki and
Raymo, 2005). Tie points are shown by triangles. WIND 28K data are from McCave
et al., (2005), ODP 806 data are from Bickert et al., (1993) and this study, and
TT013-PC72 data are from Murray et al., (2000). Open symbols show published data
and filled symbols show new data.

861

862

863

864 **Supplementary material references**

- 865 Allen, K., Hönisch, B., Eggins, S.M., Rosenthal, Y., 2012. Environmental controls on B/Ca
866 in calcite tests of the tropical planktic foraminifer species *Globigerinoides ruber* and
867 *Globigerinoides sacculifer*. *Earth Planet. Sci. Lett.* 351, 270–280.
868 doi:10.1016/j.epsl.2012.07.004
- 869 Anderson, R.F., Fleisher, M.Q., Lao, Y., Winckler, G., 2008. Modern CaCO₃ preservation in
870 equatorial Pacific sediments in the context of late-Pleistocene glacial cycles. *Mar.*
871 *Chem.* 111, 30–46. doi:10.1016/j.marchem.2007.11.011
- 872 Barker, S., Greaves, M., Elderfield, H., 2003. A study of cleaning procedures used for
873 foraminiferal Mg/Ca paleothermometry. *Geochemistry Geophys. Geosystems* 4, 1–20.
874 doi:10.1029/2003GC000559
- 875 Bickert, T., Berger, H., Burke, S., Schmidt, H., Wefer, G., 1993. Late Quaternary Stable
876 Isotope Record of Benthic Foraminifers: Site 805 and 806, Ontong Java Plateau. *Proc.*
877 *Ocean Drill. Program, Sci. Results* 411–420.
- 878 Coadic, R., Bassinot, F., Dissard, D., Douville, E., Greaves, M., Michel, E., 2013. A core-top
879 study of dissolution effect on B/Ca in *Globigerinoides sacculifer* from the tropical
880 Atlantic: Potential bias for paleo-reconstruction of seawater carbonate chemistry.
881 *Geochemistry, Geophys. Geosystems* 14, 1053–1068. doi:10.1029/2012GC004296
- 882 Johnstone, H.J.H., Kiefer, T., Elderfield, H., Schulz, M., 2014. Calcite saturation,
883 foraminiferal test mass, and Mg/Ca-based temperatures dissolution corrected using
884 XDX-A 150 ka record from the western Indian Ocean. *Geochemistry Geophys.*
885 *Geosystems* 15, 781–797. doi:10.1002/2013GC004994
- 886 Lisiecki, L.E., Raymo, M.E., 2005. A Pliocene-Pleistocene stack of 57 globally distributed
887 benthic $\delta^{18}\text{O}$ records. *Paleoceanography* 20, 1–17. doi:10.1029/2004PA001071
- 888 McCave, I.N., Kiefer, T., Thornalley, D.J.R., Elderfield, H., 2005. Deep flow in the
889 Madagascar-Mascarene Basin over the last 150,000 years. *Philos. Trans. A. Math.*
890 *Phys. Eng. Sci.* 363, 81–99. doi:10.1098/rsta.2004.1480
- 891 Medina-Elizalde, M., Lea, D.W., 2005. The mid-Pleistocene transition in the tropical Pacific.
892 *Science* 310, 1009–1012. doi:10.1126/science.1115933
- 893 Misra, S., Greaves, M., Owen, R., Kerr, J., Elmore, A.C., Elderfield, H., 2014. Determination
894 of B/Ca of natural carbonates by HR-ICP-MS. *Geochemistry, Geophys. Geosystems*
895 15, 1617–1628. doi:10.1002/2013GC005049
- 896 Murray, R.W., Knowlton, C., Leinen, M., Mix, A., Polsky, C., 2000. Export production and
897 terrigenous matter in the Central Equatorial Pacific Ocean during interglacial oxygen
898 isotope Stage 11. *Glob. Planet. Change* 24, 59–78. doi:10.1016/S0921-
899 8181(99)00066-1
- 900 Murray, R.W., Leinen, M., Murray, D.W., Mix, A.C., Knowlton, C.W., 1995. Terrigenous Fe

901 input and biogenic sedimentation in the glacial and interglacial equatorial Pacific
902 Ocean. *Global Biogeochem. Cycles* 9, 667–684. doi:10.1029/95GB02833

903 Rae, J.W.B., Foster, G.L., Schmidt, D.N., Elliott, T., 2011. Boron isotopes and B/Ca in
904 benthic foraminifera: Proxies for the deep ocean carbonate system. *Earth Planet. Sci.*
905 *Lett.* 302, 403–413. doi:10.1016/j.epsl.2010.12.034

906 Yu, J., Anderson, R.F., Jin, Z., Rae, J.W.B., Opdyke, B.N., Eggins, S.M., 2013. Responses
907 of the deep ocean carbonate system to carbon reorganization during the Last Glacial–
908 interglacial cycle. *Quat. Sci. Rev.* 76, 39–52. doi:10.1016/j.quascirev.2013.06.020

909 Yu, J., Broecker, W.S., Elderfield, H., Jin, Z., McManus, J., Zhang, F., 2010. Loss of carbon
910 from the deep sea since the Last Glacial Maximum. *Science* 330, 1084–1087.
911 doi:10.1126/science.1193221

912 Yu, J., Day, J., Greaves, M., Elderfield, H., 2005. Determination of multiple element/calcium
913 ratios in foraminiferal calcite by quadrupole ICP-MS. *Geochemistry, Geophys.*
914 *Geosystems* 6, GC000964. doi:10.1029/2005GC000964

915 Yu, J., Elderfield, H., 2007. Benthic foraminiferal B/Ca ratios reflect deep water carbonate
916 saturation state. *Earth Planet. Sci. Lett.* 258, 73–86. doi:10.1016/j.epsl.2007.03.025

917
918
919
920
921
922